Intensity difference squeezing of high-power modes in a strongly overcoupled silicon nitride microresonator

SARA PERSIA[1,*], YI SUN[1], VAISHALI ADYA[2], AND VICTOR TORRES-COMPANY[1]

[1] Department of Microtechnology and Nanoscience (MC2), Photonics Laboratory, Chalmers University of Technology, SE-41296 Göteborg, Sweden
[2] Department of Applied Physics, KTH Royal Institute of Technology, SE-106 91 Stockholm, Sweden
[*] persias@chalmers.se

Compiled February 8, 2026

Integrated nonlinear microring resonators are promising sources of bright twin-beams exhibiting intensity difference squeezing. To take advantage of the noise reduction of these quantum states, many applications require high squeezing levels in high-power mode pairs. However, the attainable on-chip squeezing is constrained by the ratio of intrinsic to coupling loss, strongly related to design and fabrication limits. Here, we demonstrate a silicon nitride microring resonator engineered to enable only a few strongly overcoupled resonances from which we directly measure 1.4 ± 0.2 dB of squeezing. The inferred on-chip intensity difference squeezing level is 11.8 dB, exceptionally high for an integrated device. In addition, the new design inherently suppresses mode competition in all other modes, enabling high power in the squeezed mode pair. These results represent a significant step toward the miniaturization of integrated devices whose performance benefits from surpassing the quantum noise limit using squeezed states, with particular relevance to sensing applications.

http://dx.doi.org/10.1364/ao.XX.XXXXXX

The main characteristic of squeezed states of light is the reduction of noise in one of the quadratures of a conjugate pair below the quantum noise limit of the vacuum state [1]. This nonclassical property offers significant technological advantages in several fields of research, from continuous variable quantum computing [2, 3] to sensing [4] and spectroscopy [5]. The most relevant example is the increased sensitivity achieved at the laser interferometer gravitational-wave observatory, where bulk optical cavities are employed to generate and control frequency-dependent squeezed vacuum states [6, 7]. So far, high levels of squeezing have been demonstrated mainly in bulk systems [8–10], with the current record of 15 dB obtained from a periodically poled KTP crystal-based optical parametric amplifier (OPA) [11].

Nevertheless, growing interest is directed toward the use of photonic integrated circuits (PICs) as squeezing sources because of their advantages in scalability, small footprint, and low power consumption. Since squeezed states require a nonlinear process to be generated from a classical coherent light, χ^2 and χ^3 nonlinear materials are commonly used in PICs devices, such as thin film lithium niobate ($LiNbO_3$) OPAs [12, 13] and silicon nitride (Si_3N_4) optical parametric oscillators (OPOs). In particular, because of their low propagation loss, strong χ^3 nonlinearity, and compatibility with complementary metal-oxide semiconductor (CMOS), Si_3N_4 microring resonators have been widely employed to generate squeezed vacuum [14–17], quantum squeezed combs [18, 19], and intensity difference squeezing [14, 20–23].

The latter is produced by pumping an OPO above the oscillation threshold P_{th}, enabling the growth of new frequency modes generated in signal-idler pairs according to the four wave mixing (FWM) process. These bright twin-beams exhibit intensity difference noise below the vacuum noise level [24, 25]. This type of squeezing is especially promising in sensing applications to enhance the sensitivity and improve the signal-to-noise ratio [26–29], and where high optical power is required for interaction with samples [4, 30].

The detectable intensity difference squeezing level generated in Si_3N_4 microresonators is [24]

$$S = 10\log_{10}(1 - \eta_{\text{path}}\eta_{\text{D}}\theta) \quad \textbf{(1)}$$

where η_{path} and η_{D} are the path and detection quantum efficiencies, respectively, and $\theta = 1 - \frac{Q_{\text{L}}}{Q_{\text{i}}}$ is the overcoupling coefficient, with Q_{L} and Q_{i} being the loaded and intrinsic quality factors. Eq.1 is valid when the product between the photon cavity lifetime τ_{c} and the measurement sideband frequency Ω is $\tau_{\text{c}}\Omega \ll 1$. The achievable on-chip squeezing $S_{\text{on-chip}}$, obtained from Eq.1 with $\eta_{\text{path}} = \eta_{\text{D}} = 1$, depends exclusively on the ratio of intrinsic to extrinsic quality factors ($Q_{\text{i}}/Q_{\text{e}}$), with maximum values achieved in the strongly overcoupled regime $Q_{\text{i}}/Q_{\text{e}} \gg 1$, where propagation losses are much lower than coupling losses [24]. Reaching this regime is nontrivial because of fabrication limits. A small Q_{e} is achieved by reducing the bus-ring waveguides gap. However, difficulties in controlling the aperture of such small gaps lead to an increase in the total intrinsic loss due to higher sidewall roughness [31]. Keeping high Q_{i} and low Q_{e} at the same time is therefore challenging. A further limitation in typical high Q_{i} resonators is the onset of oscillations of several frequency modes from high-order FWM even at moderate pump power. This causes mode competition and therefore reduces the maximum power that twin-beams can sustain while maintaining high levels of squeezing. So far, the highest reported

signal-idler power in a microresonator is a few mW for an inferred on-chip squeezing of 4.9 dB [22]. Similar issues for high Q_i microrings operating in the classical regime, such as in high power OPO for laser applications, have previously been overcome in our group by engineering the microring design so that periodic supermodes with an extremely high Q_i/Q_e ratio can be created [31, 32]. In this letter, we use the strongly overcoupled resonances of these devices to show on-chip intensity difference squeezing of 11.8 dB from twin-beams that can reach up to 7 dBm of on-chip power while still suppressing mode competition.

For this demonstration, we fabricate a Si_3N_4 microresonator embedded in SiO_2 using a subtractive process [33, 34]. The ring has a radius of 227.8 µm, corresponding to a free spectral range (FSR) of 100 GHz. As shown in the schematic in Fig.1 a), both the ring and the bus waveguide have a 740×2400 nm^2 cross section, supporting the propagation of the fundamental TE_{00} mode and the first higher-order TE_{10} mode. The bus waveguide ends are tapered to improve fiber-to-chip coupling and to ensure the excitation of only the TE_{00} mode. The gap between the bus and the ring waveguides is reduced to 120 nm. This small separation allows for the coupling between the fundamental cavity mode and both bus modes, thereby increasing the total intrinsic loss of the device. However, at the Vernier frequencies of the TE_{00} and TE_{10} resonances, destructive interference of common loss mechanisms can suppress the total loss, resulting in the formation of high Q_i supermodes described as quasi bound states in the continuum (quasi-BICs) [32].

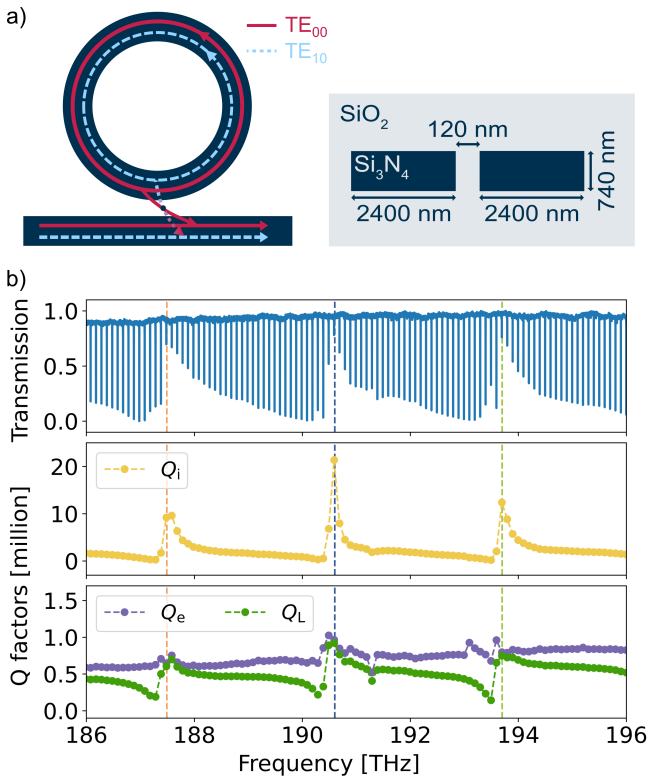

Fig. 1. a) Schematic and cross section of the Si_3N_4 microring resonator. The large waveguide dimension combined with the small gap let quasi-BICs modes to arise. b) Frequency dependent periodic normalized transmission spectrum and Q factors distribution. The dashed lines indicate the strongly overcoupled resonances used as signal (orange), pump (blue), and idler (light green) modes.

We characterize the cold cavity properties of this device using sweep wavelength interferometry [35]. This technique enables the retrieval of the amplitude and phase of every longitudinal mode, hence allowing to unambiguously identify their coupling regimes. The normalized transmission spectrum and the extracted quality (Q) factors shown in Fig.1 b) exhibit periodic patterns with period equal to 31 FSRs, indicating that only a small number of cavity modes in the C+L optical band are strongly overcoupled and therefore capable of supporting high squeezing generation. All other modes are characterized by low Q_i, suppressing cascade FWM even for high-power signal-idler pairs [31]. The central mode highlighted with the blue dashed line in Fig.1 b) is used as the pump, at frequency $\omega_p = 2\pi \times 190.59$ THz. The first signal and idler modes are expected to appear at $\omega_s = 2\pi \times 187.48$ THz and $\omega_i = 2\pi \times 193.70$ THz, respectively, due to the position of the strongly overcoupled modes and the energy and momentum conservation that must be fulfilled by FWM. We calculate the overcoupling coefficients for these modes to be $\theta_s = 0.934$ and $\theta_i = 0.939$. The difference in the Q factors, and consequently in the θ values, is the first source of squeezing degradation, as it represents different photon losses experienced by the two beams during propagation in the ring and in the bus-ring coupling. For this device, the idler has a lower intrinsic loss and almost the same coupling loss as the signal. Using the lowest overcoupling coefficient (θ_s) in Eq.1, we estimate an on-chip intensity difference squeezing of $S_{\text{on-chip}} = 11.8$ dB, which exceeds the previous record of 10.2 dB reported in [23]. This improvement provides increased resilience against the losses arising from the detection and possible on-chip operations.

From Eq.1, we see that the detectable squeezing level strongly depends also on the setup losses and the quantum efficiency of the detector, in addition to θ. To maximize η_{path}, we use free-space components to couple the light out of the chip and to

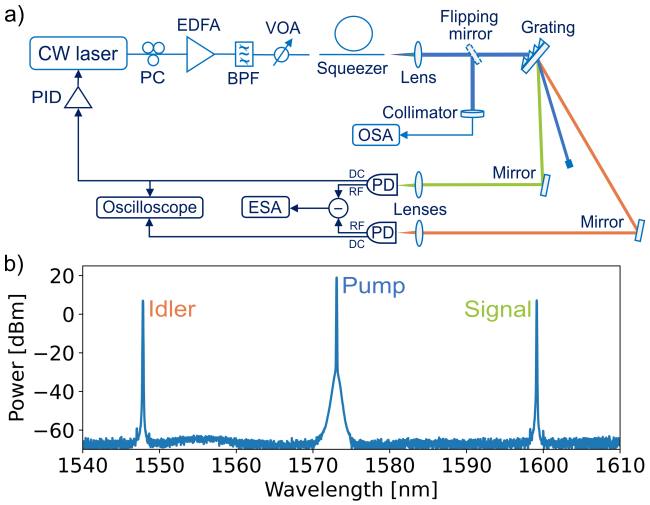

Fig. 2. a) Simplified schematic of the intensity difference squeezing measurement setup. The different signal and idler paths after the grating are highlighted in light green and orange, respectively. CW laser: continuous wave laser; EDFA: erbium doped fiber amplifier; BPF: optical band pass filter; VOA: variable optical attenuator; OSA: optical spectrum analyzer; PD: photodetector; ESA: electrical spectrum analyzer; PID: proportional-integral-derivative control. b) Optical spectrum measured with the OSA displaced to show the on-chip signal and idler high powers.

separate the modes, as shown in the experimental setup in Fig.2 a). In particular, an aspheric lens collects the output light, reducing the facet coupling loss to 0.8 dB compared to 2.98 dB of fiber-to-chip input loss. Then, a transmission grating spatially separates the three main frequency components, and a series of mirrors and lenses direct and focus the signal and idler beams onto the two ports of the balanced photodetector (BPD). As a consequence of the fixed position of the strongly overcoupled resonances, the large frequency distance between the signal and the idler resonances of about 50 nm, shown in Fig.2 b), facilitates the spatial separation of the modes. This reduces the total number of components necessary to create the two different parallel paths towards the BPD and the physical distance between the chip and the detector, consequently limiting the total path loss.

During the noise measurement, it is crucial to balance the two PDs by equalizing their photocurrents. These are monitored on an oscilloscope via the DC output ports of the BPD. Because of the unequal Q factors and the frequency dependent losses of the components, the signal and idler powers are not identical. We correct this imbalance by intentionally increasing the path loss of the higher power beam. After balancing the PDs, the total path efficiency is $\eta_{\text{path}} = 0.46$, including also the loss due to focusing the beams into the small active area of the free-space BPD, whose quantum efficiency is measured to be $\eta_{\text{D}} = 0.688$. To maintain constant signal and idler powers during the squeezing measurement, we use the DC photocurrent generated by the signal beam as the error signal of a PID control loop that directly changes the pump laser wavelength. A flipping mirror placed after the aspheric lens directs the light into an OSA used for monitoring of the output optical spectrum. By sweeping the laser-resonance frequency detuning while pumping the microring with 19.5 dBm of on-chip power, we generate signal and idler modes that can reach approximately 7 dBm of on-chip power before the onset of high-order FWM. This is shown in Fig.2 b). However, such high signal-idler power is not reached during the actual intensity difference squeezing measurement because of the saturation of the BPD used in the power stabilization loop.

Intensity difference squeezing is analyzed by comparing the noise power of the photocurrent difference generated in the BPD with the shot noise of the pump laser at frequency ω_p with a power equal to the average signal-idler power. We previously verified that the entire setup operates at the shot noise limit by measuring the linear dependence of the noise power on the input laser power. The noise spectra measured with the ESA are shown in Fig.3 a). We observe squeezing across the entire BPD frequency bandwidth, starting from approximately 5 MHz. At lower frequencies, the technical noise from the laser and the BPD, as well as the additional noise due to the beam power unbalancing, dominates over the detectable squeezing. The shape of the measured curves resembles that of the dark noise spectrum of the BPD, which remains below the measured shot noise. To accurately characterize the intensity difference squeezing level, we perform the zero-span measurement shown in Fig.3 b). We choose $\Omega = 2\pi \times 10$ MHz to stay within the frequency range where Eq.1 is valid. We directly measure $S_{\text{meas}} = 1.4 \pm 0.2$ dB of squeezing, mainly limited by the quantum efficiency of the PDs and the losses associated with focusing the beams in the BPD. The uncertainty of the squeezing measurement comes from the accuracy of the ESA. The consistency of this squeezing level throughout the measurement time of 24 s is ensured by the stabilization of the signal-idler power.

From this value, and taking into account η_{path} and η_{D} measured previously, we can calculate the corresponding on-chip squeezing $S'_{\text{on-chip}}$ generated in the bus waveguide. We model the effect of the total setup loss $\eta = \eta_{\text{path}}\eta_{\text{D}}$ with the typical beam splitter relation [36]

$$V_{\text{meas}} = \eta V_{\text{on-chip}} + (1-\eta)V_{\text{vac}}, \tag{2}$$

where we assume to have in one input port the variance of the on-chip squeezing $V_{\text{on-chip}}$ and in the other port the variance of the vacuum state V_{vac}, equal to 1 by definition. The variance of the measured squeezing is obtained at the output transmission port. We calculate $S'_{\text{on-chip}} = 10\log_{10}(V_{\text{on-chip}}) = 9.2 \pm 5.1$ dB, in agreement with the inferred $S_{\text{on-chip}}$ obtained from the analysis of the Q factors. The large uncertainty on $S'_{\text{on-chip}}$ is obtained from the error propagation analysis and is mainly due to the measurement uncertainty of the power values used to estimate η and the uncertainty of the measured squeezing level. The comparison between $S'_{\text{on-chip}}$ and S_{meas} highlights the nonlinear worsening effect of loss on the detectable squeezing level. Nevertheless, for integrated squeezing sources, the key result is the high level of on-chip squeezing enabled by our engineered microring design because of the strongly overcoupling regime reached in the pump, signal, and idler resonance modes. These results represent a high-record value of intensity difference squeezing generated on-chip in PICs.

According to Eq.1, the intensity difference squeezing level generated above P_{th} remains constant for any mode power, in contrast to vacuum squeezing that reaches its maximum close to the threshold [24]. Therefore, we investigate the stability of

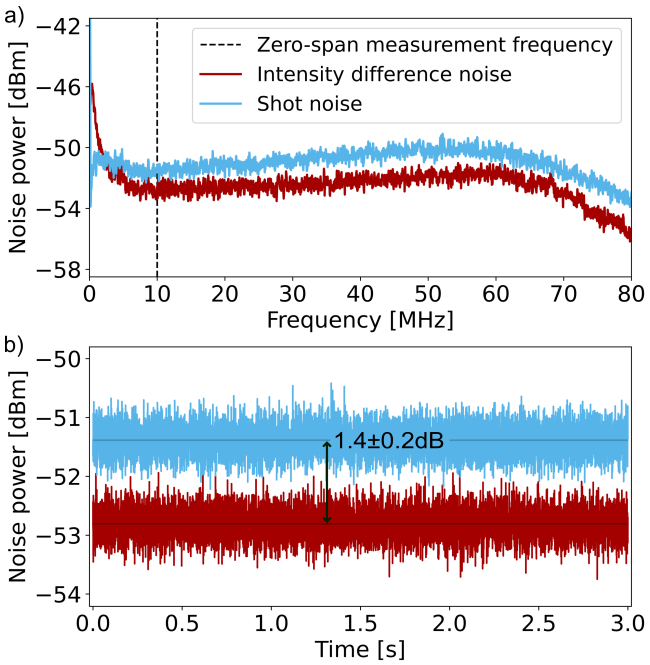

Fig. 3. a) Comparison between the intensity difference noise power (red) and the shot noise (ligh blue) within the BPD RF frequency range. Below 5 MHz, technical noise prevails over squeezing. b) Zero-span measurement of intensity difference squeezing performed at 10 MHz. The signal and idler average power is −4.6 dBm and the measured squeezing level is 1.4 ± 0.2 dB. Data shown in a) and b) are collected using the ESA with resolution bandwidth of 100 kHz and video bandwidth of 3 kHz by averaging over 8 traces of 3 s each.

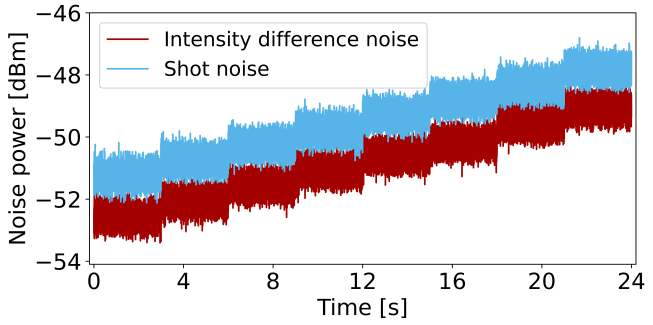

Fig. 4. Intensity difference squeezing measured in the ESA zero-span mode while subsequently increasing the signal-idler average power by effectively controlling the pump detuning with the PID feedback loop. An averaged squeezing of 1.3 ± 0.2 dB is measured during the sweep. The ESA settings are the same as for Fig.3.

the squeezing generated from our device by sweeping the average signal and idler power. The results are shown in Fig.4. In this measurement, the error signal used in the power stabilization feedback loop is gradually increased until we reach an average signal and idler power of 630 µW. This value, obtained by measuring the idler power just before detection, is limited by the maximum photocurrent generated in the monitor ports of the BPD. As shown previously in Fig.2 b), the signal and idler modes could in principle reach much higher power levels before initiating unwanted processes that could degrade the generated squeezing. The squeezing level shown in Fig.4 is constant around 1.3 ± 0.2 dB during the total acquisition time of more than 3 minutes, demonstrating high stability across a large temporal window and a broad range of mode powers suitable for many applications.

In summary, we demonstrate that quasi-BICs modes arising in an engineered Si_3N_4 microresonator enable access to the optimal coupling regime for high squeezing generation. We exploit these periodic strongly overcoupled resonances to generate high power twin-beams with an estimated record on-chip intensity difference squeezing of 11.8 dB. We also show that the signal and idler beams can reach up to 7 dBm of on-chip power before the onset of higher-order FWM processes. Furthermore, we show the potential of this new design to provide stable squeezing over at least 3 min in a high-power mode pair with large wavelength separation of about 50 nm, facilitating the spatial separation of the signal and idler modes. Further improvements in the achievable on-chip intensity difference squeezing level can be obtained by reducing even more the gap between the ring and the bus waveguides, thus increasing θ. As shown in [31], the enhancement of the overcoupling coefficient also allows higher signal and idler powers to be achieved. These improvements can be beneficial for several applications, specially in sensing, where stability and control over the twin-beams power and spectral separation can be critical.

Funding. Knut and Alice Wallenberg foundation via the Wallenberg Centre for Quantum Technology (WACQT); Swedish Research Council (2020-00453, 2022-0657)

Acknowledgment. The authors thank the cleanroom staff from Myfab at Chalmers Nanofabrication Laboratory.

Disclosures. The authors declare no conflicts of interest.

REFERENCES

1. A. I. Lvovsky, *Squeezed Light* (John Wiley & Sons, Ltd, 2015), chap. 5, pp. 121–163.
2. H. A. Rad, T. Ainsworth, R. N. Alexander, *et al.*, Nature **638**, 912 (2025).
3. P. Marek, Phys. Rev. Lett. **132**, 210601 (2024).
4. B. J. Lawrie, P. D. Lett, A. M. Marino, and R. C. Pooser, ACS Photonics **6**, 1307 (2019).
5. H. Shi, Z. Chen, S. E. Fraser, *et al.*, npj Quantum Inf. **9**, 91 (2023).
6. D. Ganapathy, W. Jia, M. Nakano, *et al.*, Phys. Rev. X **13**, 041021 (2023).
7. W. Jia, V. Xu, K. Kuns, *et al.*, Science **385**, 1318 (2024).
8. G. Sim, H. Kim, and H. S. Moon, Sci. Reports **15**, 7727 (2025).
9. M. Mehmet, S. Ast, T. Eberle, *et al.*, Opt. Express **19**, 25763 (2011).
10. K. Hirota, T. Kashiwazaki, G. Ha, *et al.*, https://arxiv.org/abs/2511.15082 (2025).
11. H. Vahlbruch, M. Mehmet, K. Danzmann, and R. Schnabel, Phys. Rev. Lett. **117**, 110801 (2016).
12. X. Shi, A. A. Baiju, X. Chen, *et al.*, http://arxiv.org/abs/2508.08599 (2025).
13. H. S. Stokowski, T. P. McKenna, T. Park, *et al.*, Nat. Commun. **14**, 3355 (2023).
14. V. D. Vaidya, B. Morrison, L. G. Helt, *et al.*, Sci. Adv. **6**, eaba9186 (2020).
15. Y. Zhao, Y. Okawachi, J. K. Jang, *et al.*, Phys. Rev. Lett. **124**, 193601 (2020).
16. Y. Zhang, M. Menotti, K. Tan, *et al.*, Nat. Commun. **12**, 2233 (2021).
17. A. E. Ulanov, B. Ruhnke, T. Wildi, and T. Herr, Nat. Commun. **16**, 10791 (2025).
18. M. Jahanbozorgi, Z. Yang, S. Sun, *et al.*, Optica **10**, 1100 (2023).
19. Y. Shen, P.-Y. Hsieh, D. Srinivasan, *et al.*, http://arxiv.org/abs/2505.03734 (2025).
20. A. Dutt, K. Luke, S. Manipatruni, *et al.*, Phys. Rev. Appl. **3**, 044005 (2015).
21. A. Dutt, S. Miller, K. Luke, *et al.*, Opt. Lett. **41**, 223 (2016).
22. R. A. Kögler, G. C. Rickli, R. R. Domeneguetti, *et al.*, Opt. Lett. **49**, 3150 (2024).
23. Y. Shen, P.-Y. Hsieh, S. K. Sridhar, *et al.*, Optica **12**, 302 (2025).
24. Y. K. Chembo, Phys. Rev. A **93**, 033820 (2016).
25. N. Quesada, L. G. Helt, M. Menotti, *et al.*, Adv. Opt. Photonics **14**, 291 (2022).
26. C. A. Casacio, L. S. Madsen, A. Terrasson, *et al.*, Nature **594**, 201 (2021).
27. F. Li, T. Li, M. O. Scully, and G. S. Agarwal, Phys. Rev. Appl. **15**, 044030 (2021).
28. T. Li, F. Li, X. Liu, *et al.*, Optica **9**, 959 (2022).
29. W. Yang, W. Diao, C. Cai, *et al.*, Chemosensors **11**, 18 (2023).
30. M. A. Taylor, J. Janousek, V. Daria, *et al.*, Nat. Photonics **7**, 229 (2013).
31. Y. Sun, F. Lei, Y. Gao, and V. Torres-Company, Opt. Lett. **50**, 4798 (2025).
32. F. Lei, Z. Ye, K. Twayana, *et al.*, Phys. Rev. Lett. **130**, 093801 (2023).
33. Z. Ye, K. Twayana, P. A. Andrekson, and V. Torres-Company, Opt. Express **27**, 35719 (2019).
34. M. Girardi, Óskar B. Helgason, C. H. López-Ortega, *et al.*, Opt. Express **33**, 27451 (2025).
35. K. Twayana, Z. Ye, Óskar B. Helgason, *et al.*, Opt. Express **29**, 24363 (2021).
36. H.-A. Bachor and T. C. Ralph, *Squeezing experiments* (John Wiley & Sons, Ltd, 2004), chap. 9, pp. 232–309.